We are IntechOpen,
the world's leading publisher of
Open Access books
Built by scientists, for scientists

6,900
Open access books available

186,000
International authors and editors

200M
Downloads

154
Countries delivered to

Our authors are among the

TOP 1%
most cited scientists

12.2%
Contributors from top 500 universities

CLARIVATE ANALYTICS
BOOK CITATION INDEX
INDEXED

WEB OF SCIENCE™

Selection of our books indexed in the Book Citation Index
in Web of Science™ Core Collection (BKCI)

Interested in publishing with us?
Contact book.department@intechopen.com

Hydrogen Reduced Rutile Titanium Dioxide Photocatalyst

Fumiaki Amano

Additional information is available at the end of the chapter

Abstract

For TiO_2 photocatalysts, recombination of photoexcited electrons and holes would occur in crystalline defects such as oxygen vacancies, Ti^{3+} ions, and surface states. Therefore, it is believed that the density of crystalline defects should be decreased to improve the photocatalytic activity of TiO_2 particles. Contrary to this common knowledge, the introduction of crystalline defects by hydrogen reduction treatment is shown to increase the lifetime of photoexcited electrons in rutile TiO_2 photocatalysts with an increase of n-type electrical conductivity. The photocatalytic activities of H_2-reduced rutile TiO_2 were higher than those of anatase TiO_2 and mixed-phase TiO_2. This chapter explains the effect of donor doping on the photocatalytic activity of rutile TiO_2, the relationship between its physicochemical properties and photocatalytic performances, and the mechanism of the enhanced activity of H_2-reduced TiO_2. Particle size dependence on the enhanced activities suggests the formation of a space charge layer in large TiO_2 crystallites.

Keywords: rutile, n-type semiconductor, conduction electron, donor density, oxygen vacancy

1. Introduction

For utilization of light energy including solar light, the development of highly active photocatalytic materials is expected. Mainly oxide photocatalysts have been studied so far, but the design guideline did not become clear even in the case of representative TiO_2. In crystalline type of TiO_2 photocatalysts such as anatase, rutile, and brookite, it is believed that anatase TiO_2 is active based on the studies such as the oxidative degradation of organic compounds, H_2 evolution from water, and photoinduced super hydrophilicity. When anatase TiO_2 is annealed to decrease the density of crystalline defects, the crystal structure is transformed into a thermodynamically stable rutile phase. Generally speaking, the photocatalytic performance of rutile-type

TiO_2 is inferior except for the case in specific photocatalyst reactions. The reasons of lower activity are attributed to the smaller BET-specific surface area, the energetically lower conduction band bottom, and the shorter lifetime of the photoexcited carriers, compared to those of anatase TiO_2.

When oxide photocatalyst absorbs light with energy larger than the bandgap, an electron is excited to the conduction band, and a positive hole generates in the valence band. The lifetime of the photoexcited electron and the hole must be long enough to promote reductive and oxidative reactions on the surface efficiently. However, most of the photoexcited carriers are deactivated by recombination at crystalline defects such as impurities and disorder of the atomic arrangement in the bulk, on the surface, and at the interface. Therefore, highly crystalline particles are considered to show high photocatalytic activity if the band structure and the BET-specific surface area are the same.

The photocatalytic activity of rutile TiO_2 is frequently low compared to that of anatase TiO_2 photocatalyst. However, Maeda recently revealed that a rutile TiO_2 can induce overall water splitting to evolve H_2 and O_2 under UV irradiation [1]. We have also found that photocatalytic activity of rutile TiO_2 was improved by H_2 reduction treatment. The reaction can be written using Kröger-Vink notation (**Table 1**). Hydrogen reduction of TiO_2 creates both oxygen vacancy and electrons as shown in Eq. (1). Therefore, this treatment is recognized as a donor doping. The electron is trapped in a Ti^{4+} lattice site to form Ti^{3+} ions (Eq. (2)). The enhanced activity by introducing lattice defects is against the common knowledge in photocatalyst chemistry: crystalline defects should be decreased.

$$O_O^\times + H_2 \rightarrow V_O^{\bullet\bullet} + 2e' + H_2O \tag{1}$$

$$Ti_{Ti}^\times + e' = Ti'_{Ti} \tag{2}$$

Despite the reputed lower activity of rutile TiO_2 than anatase, it is important to determine the physical properties affecting the photocatalytic efficiency of rutile TiO_2. This chapter explains the donor doping effect on rutile TiO_2 photocatalysts and the effect of H_2 reduction treatment

Notation	Meaning
$Ti_{Ti}^\times$	Ti^{4+} ion in titanium lattice site
M'_{Ti}	M^{3+} ion in titanium lattice site
$M_{Ti}^\bullet$	M^{5+} ion in titanium lattice site
e'	Conduction electron
$O_O^\times$	O^{2-} ion in oxygen lattice site
$OH_O^\bullet$	OH^- ion in oxygen lattice site
$V_O^{\bullet\bullet}$	Oxygen vacancy, with double positive charge

Note: **M** corresponds to metal cation.

Table 1. Kröger-Vink notation of species in TiO_2 lattice.

on the photocatalytic activity of rutile TiO_2. The properties of the H_2-reduced rutile TiO_2 were characterized using diffuse reflectance UV-vis-NIR spectroscopy, electron spin resonance (ESR) spectroscopy, sheet resistance measurements, and electrochemical Mott-Schottky analysis. The role of oxygen vacancies, Ti^{3+} species, and conduction band electrons in the enhancement of photocatalytic and PEC activities of H_2-reduced TiO_2 is discussed based on the experimental results.

2. Doping in oxide photocatalysts

For semiconductor materials in electronic use, the density of electrons and holes is controlled by the doping of impurities into crystalline materials. Doping means incorporation of foreign impurities into the crystalline lattice of the parent semiconductor, and it is significantly different from surface modification. The donor doping implies an introduction of electrons to create an n-type semiconductor. The n-type conductivity is increased by donor doping and decreased by an acceptor doping-introducing hole. The electrons in the conduction band and the trapping site are one of crystalline defects in a wide meaning.

In semiconductor photocatalysts, doping of impurities is used to control the band structures. An impurity level and a subband can be formed in the bandgap by substituting a different ion for an ion constituting a crystal, and it is applied for the development of visible light-responsive photocatalysts. However, photocatalytic activity under visible-light irradiation has not yet been in practical use because of the low quantum yield. The doped impurities frequently resulted in deactivation of the doped photocatalysts, suggesting that the dopants and the created defects work as a recombination center decreasing the lifetime of photoexcited electrons and holes.

2.1. Perovskite oxide photocatalysts

There are many papers reporting the enhancement of photocatalytic activity by doping of cations and anions, although some of the reports lack reproducibility and experimental evidence. For perovskite oxide photocatalysts, some research groups reported that the photocatalytic activity was enhanced by acceptor doping, that is, doping of cations with valence lower than that of the parent cations. It is known that oxygen vacancies are easily formed in perovskite oxides, which resulted in the increase of electron density (Eq. (3)) and the origin of n-type semiconductivity.

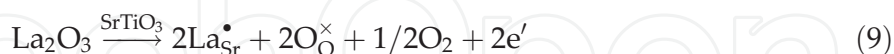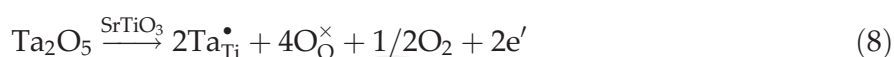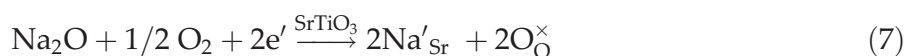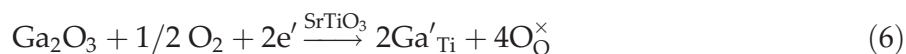$$O_O^\times \rightarrow V_O^{\bullet\bullet} + 2e' + 1/2\,O_2 \tag{3}$$

The electrons are trapped in shallow midgap states near conduction band bottom and can be easily excited from the donor levels to the conduction band. During photoexcitation, photogenerated holes would recombine with the electrons in addition to the photoexcited electrons. Therefore, a higher accumulation of electrons in n-type oxide would result in lower photocatalytic activity. Actually, this is true for perovskite oxide photocatalysts such as $SrTiO_3$ and $KTaO_3$ [2–4].

Ishihara et al. reported that the doping of Zr^{4+} to $KTaO_3$ particles was effective for improving the activity for overall water splitting under UV irradiation [2, 3]. The photocatalytic activity of nondoped $KTaO_3$ loaded with a NiO cocatalyst ($NiO/KTaO_3$) was negligible, but the doping of a small amount of tetravalent cations such as Zr^{4+} increases the rate of photocatalytic H_2 and O_2 evolution. $KTaO_3$ was originally an n-type semiconductor, since the electrical conductivity was monotonically increased with decreasing oxygen partial pressure. The doping of acceptors would decrease electron density in $KTaO_3$ according to Eqs. (4) and (5). The electrical conductivity of $KTaO_3$ was decreased with an increase of the amount of doped Zr^{4+}, which resulted in the enhanced photocatalytic activity.

$$ZrO_2 \xrightarrow{KTaO_3} Zr'_{Ta} + 2O_O^{\times} + 1/2V_O^{\bullet\bullet} \tag{4}$$

$$V_O^{\bullet\bullet} + 1/2\,O_2 + 2e' \rightarrow O_O^{\times} \tag{5}$$

Takata and Domen also reported that acceptor doping effectively enhanced the photocatalytic activity of cocatalyst-loaded $SrTiO_3$ particles for overall water splitting [4]. Ga-doped and Na-doped $SrTiO_3$ exhibited photocatalytic activity higher than that of nondoped $SrTiO_3$ by about 10 times. Ga^{3+} occupies the Ti^{4+} site and Na^+ occupies the Sr^{2+} site, which resulted in the decrease of electron concentration (Eqs. (6) and (7)). In contrast, the doping of a higher valence cations (Ta and La) led to the suppressed photocatalytic activity of $SrTiO_3$ (Eqs. (8) and (9)). Here, Ta^{5+} occupies Ti^{4+} site, and La^{3+} occupies the Sr^{2+} site increasing the electron density of $SrTiO_3$. Since the electrons are trapped in Ti^{4+} sites to create Ti^{3+} species (Eq. (2)), the defect species most responsible for recombination would be Ti^{3+} species in n-type perovskite oxide photocatalysts.

$$Ga_2O_3 + 1/2\,O_2 + 2e' \xrightarrow{SrTiO_3} 2Ga'_{Ti} + 4O_O^{\times} \tag{6}$$

$$Na_2O + 1/2\,O_2 + 2e' \xrightarrow{SrTiO_3} 2Na'_{Sr} + 2O_O^{\times} \tag{7}$$

$$Ta_2O_5 \xrightarrow{SrTiO_3} 2Ta_{Ti}^{\bullet} + 4O_O^{\times} + 1/2O_2 + 2e' \tag{8}$$

$$La_2O_3 \xrightarrow{SrTiO_3} 2La_{Sr}^{\bullet} + 2O_O^{\times} + 1/2O_2 + 2e' \tag{9}$$

2.2. TiO_2 photocatalysts

The roles of dopants in TiO_2 photocatalysts are complicated and controversial, since it might depend on the particle size, the crystallinity, the crystalline phase, and reaction conditions. Generally speaking, impurities and crystalline defects work as recombination centers. However, there are some reports pointing that donor doping enhanced the photocatalytic activity of Pt-loaded TiO_2 [5, 6]. This trend for Pt/TiO_2 photocatalysts is opposite to the case of perovskite oxides, which is activated by acceptor doping.

Karakitsou and Verykios reported the effect of aliovalent cation doping to the TiO_2 matrix on the photocatalytic activity of Pt/TiO_2 for H_2 evolution [5]. Since the doped TiO_2 was prepared at 900°C, the crystalline structure was rutile phase and the particle size was large (BET-specific

surface area, ~1 m^2 g^{-1}). In contrast to the case of perovskite oxides mentioned above, the doping of cations with valence higher than Ti^{4+} (W^{6+}, Ta^{5+}, and Nb^{5+}) enhanced the photocatalytic activity, while the opposite was observed for acceptor doping (In^{3+}, Zn^{2+}, and Li^+). The measurement of electrical conductivity revealed that the cation doping changed the bulk electronic structure [7]. The authors concluded that n-type conductivity correlates with the enhanced photocatalytic activity of Pt/TiO_2 with rutile form.

Ying et al. investigated the role of particle size in cation-doped TiO_2 nanoparticles with anatase crystalline structure [6]. For TiO_2 nanocrystals with an average diameter less than 11 nm, the doping of Fe^{3+} enhanced the photocatalytic activity for $CHCl_3$ degradation. The optimal concentration of Fe^{3+} dopants decreased with increasing TiO_2 particle size, suggesting that the role of Fe^{3+} species is the inhibition of surface recombination. The Fe^{3+} doping might work less effectively for large TiO_2 particles, since the dominant recombination process is bulk recombination rather than surface recombination. The photocatalytic activity of TiO_2 with large particle size was increased by Nb^{5+} doping in a combination with Pt loading, while the activity was decreased by sole Nb^{5+} doping.

3. Deactivation of TiO_2 photocatalysts at high temperature

Improving crystallinity by annealing can enhance the photocatalytic activity of TiO_2 by decreasing defects that act as recombination centers. However, high temperature calcination frequently decreased photocatalytic activity. This deactivation is commonly attributed to a change of the crystal structure from anatase to rutile and a decrease in BET-specific surface area because of crystal growth. Both crystallinity and specific surface area, which are related to particle size, are changed by high temperature calcination. Therefore, it is difficult to characterize the effect of annealing except for the effects by crystal growth.

We investigated the effect of high temperature calcination on the photocatalytic activity of rutile TiO_2 with a small BET-specific surface area, ~2.3 m^2 g^{-1}, to diminish the change in the crystalline phase and surface area by crystal growth [8]. Photocatalytic activity toward H_2 evolution was examined using an aqueous ethanol solution, with *in-situ* photodeposited Pt nanoparticles, under UV irradiation. **Figure 1** shows that the rate of photocatalytic H_2 evolution was significantly decreased by calcination in air at temperatures higher than 500°C, although the BET-specific surface area showed a little change. These results indicated that the deactivation of rutile TiO_2 particles at high temperature calcination could not be attributed to the phase transition and the decreased surface area.

Then, the behavior of photoexcited electrons was examined using transient IR spectroscopy to probe the dynamics of photoexcited electrons [8]. Changes in IR absorption were recorded after the pump irradiation of 355-nm laser pulse in the presence of methanol. Owing to low signal levels under vacuum, methanol was added as an electron donor. **Figure 2** shows the millisecond-scale decay of the photoinduced IR absorption observed for calcined rutile samples. Since the photogenerated holes react with methanol within a millisecond, the decay of the signal attributed to photoexcited electrons is very slow. The signal magnitude decreased as
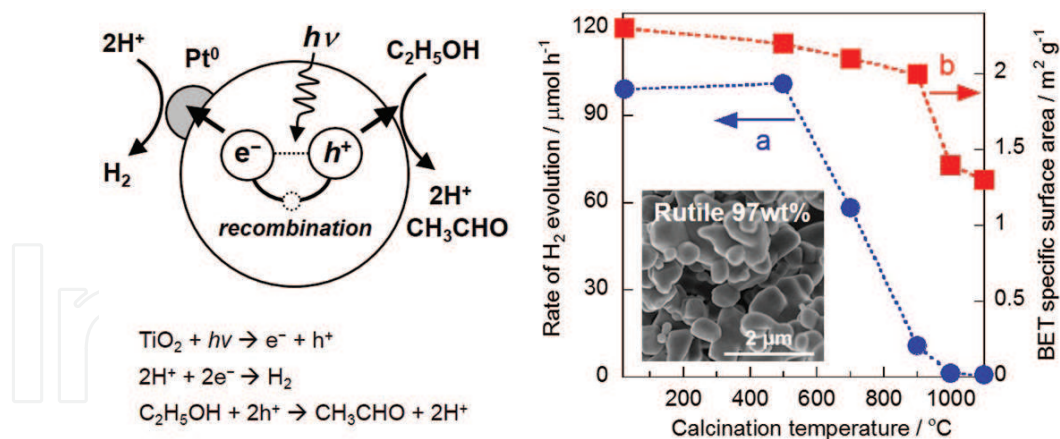
Figure 1. Effect of calcination temperature on (a) the rate of photocatalytic H_2 evolution from an aqueous solution of 50 vol% ethanol with H_2PtCl_6 (2.0 wt% as Pt) under UV irradiation from light emitting diode (peak wavelength 380 nm) and (b) BET specific surface area of rutile TiO_2 particles.
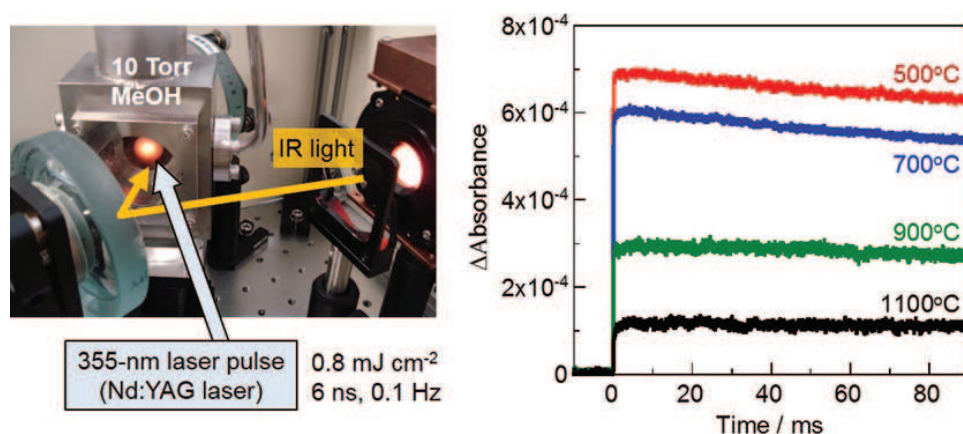
Figure 2. Transient IR spectroscopy setup and the transient absorption at 2000 cm^{-1} triggered by a 355-nm laser pulse with 6-ns duration in the presence of methanol of the rutile TiO_2 calcined in air at different temperatures: 500°C, 700°C, 900°C, and 1100°C.

calcination temperature of the sample increased, suggesting the more recombination of photo-excited carriers. The rutile TiO_2 particles calcined at high temperature showed the less density of long-lived photoexcited electrons, which resulted in the low photocatalytic activity. The reason for the deactivation at high temperature calcination is attributed to fast charge carrier recombination.

4. Hydrogen treatment of rutile TiO_2

4.1. Photocatalytic activity of reduced TiO_2

TiO_2 is often considered as a nonstoichiometric oxygen-deficient compound. According to Eq. (3), a small amount of electrons would be naturally doped. However, the n-type conductivity may be decreased by calcination in air at high temperature owing to the strong oxidation. To confirm the effect of electron density on the fast recombination observed in deactivated

TiO_2, we performed H_2 reduction treatment to the rutile TiO_2 particles calcined at 1100°C [8]. The TiO_2 samples were reduced by H_2 at 500 or 700°C, increasing both the density of long-lived charge carriers and photocatalytic activity (**Figure 3**). These results suggest that the density of oxygen vacancies and/or electrons is an important factor determining the photocatalytic activity.
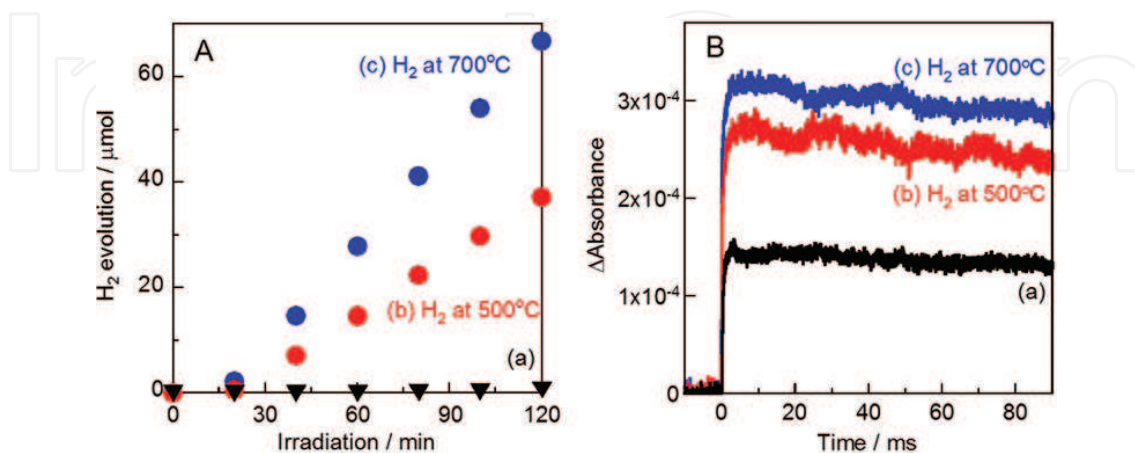
Figure 3. (A) Time course of photocatalytic H_2 evolution from an aqueous ethanol solution with Pt, and (B) transient IR absorption triggered by a 355-nm laser pulse in the presence of methanol: (a) TiO_2 calcined in air at 1100°C, (b) TiO_2 reduced with H_2 at 500°C after calcination at 1100°C, and (c) TiO_2 reduced with H_2 at 700°C after calcination at 1100°C.

H_2 reduction treatment has received extensive attention for improving the photocatalytic activity of anatase TiO_2 nanostructures since the recent report of the visible-light sensitivity of "hydrogenated black TiO_2" with defect disorders [9]. H_2 reduction treatment has also been reported to improve the PEC activity of TiO_2 nanowire arrays [10]. The H_2 treatment creates a high density of oxygen vacancies and electrons as shown in Eq. (1). We investigated the effects of H_2 treatment temperature on the photocatalytic activity of rutile TiO_2 particles to discuss the role of oxygen vacancies, Ti^{3+} ions, and conduction band electrons [11]. The photocatalytic activity was examined using an O_2 evolution from an aqueous solution of 50 mmol L^{-1} $AgNO_3$ as a sacrificial electron acceptor ($4Ag^+ + 2H_2O \rightarrow 4Ag^0 + O_2 + 4H^+$). Calcination above 900°C decreased the photocatalytic activity of rutile TiO_2 particles probably owing to strong oxidation, but its initial activity was restored by H_2 treatment at above 500°C. The photocatalytic activity of reduced TiO_2 was hardly changed after recalcination in air at 300°C, but significantly decreased after recalcination at 500°C.

4.2. ESR and UV-vis-NIR spectroscopy

Electron spin resonance (ESR) is active for paramagnetic species such as Ti^{3+} ions (electron trapped in titanium lattice site) and $O^{\bullet-}$ radicals (hole trapped in oxygen lattice site). **Figure 4A** shows ESR spectra of the H_2-reduced TiO_2 samples [11]. The TiO_2 calcined at 1100°C exhibited signals with g = 2.061 and 2.045. Kumar et al. have reported radical formation (g_1 = 2.026, g_2 = 2.017, and g_3 = 2.008) on rutile TiO_2 by calcination at 750°C and assigned the signals to trapped holes on the surface ($Ti^{4+}O^{2-}Ti^{4+}O^{\bullet-}$ radicals) [12]. It has been reported that strong oxidation of TiO_2 facilitates the transformation of n-type oxygen-deficient TiO_{2-x} to p-type metal-deficient $Ti_{1-y}O_2$ [13]. The high temperature calcination of TiO_2 may be considered

as acceptor doping to create titanium vacancy (V''''_{Ti}) and hole ($h^\bullet$) according to Eq. (10). The hole would be trapped in the oxygen lattice site as an $O^{\bullet-}$ radical.

$$O_2 \rightarrow 2O_O^\times + V''''_{Ti} + 4h^\bullet \tag{10}$$

The signals attributable to $O^{\bullet-}$ radicals (trapped hole) disappeared after H_2 treatment at 400°C, indicating that strongly oxidized $Ti_{1-y}O_2$ was reduced to neutral TiO_2 by the mild H_2 treatment. The ESR spectrum of TiO_2 reduced at 500°C exhibited a sharp signal at $g = 2.002$ assigned to electrons trapped in oxygen vacancies and an intense signal at $g = 1.974$ assigned to Ti^{3+} ions (electron trapped in Ti lattice site) in rutile. This indicates that H_2 treatment at 500°C further reduced the TiO_2 to oxygen-deficient TiO_{2-x}. The signal at $g = 1.974$ was significantly broadened when the H_2 treatment temperature was increased to 700°C, indicating the high density of Ti^{3+} ions. The TiO_2 reduced at 700°C was assumed to be deeply doped n-type TiO_2.

The color of the TiO_2 samples changed from white to a pale ash color after H_2 reduction treatment [11]. **Figure 4B** shows diffuse reflectance UV-vis-NIR spectra of the TiO_2 samples. The onset of intense photoabsorption originating from interband transitions was located at ca. 415 nm corresponding to the bandgap of rutile, 3.0 eV. The spectrum of TiO_2 reduced at 500 and 700°C exhibited a broad absorption located in the visible and NIR region, which can be assigned to the transition of electrons in shallow traps and the conduction band. From the NIR absorption, the density of electrons in the TiO_2 reduced at 500°C was higher than that in the TiO_2 reduced at 700°C. Therefore, it is concluded that H_2 reduction at higher temperature increased the density of electrons in the conduction band.

4.3. X-ray photoelectron spectroscopy (XPS)

Figure 5 shows X-ray photoelectron spectra of the strongly oxidized TiO_2 and reduced TiO_2 [11]. There was no significant change in the Ti 2p spectra. The binding energy of 458.6 eV for Ti $2p_{3/2}$ was similar to the literature value for Ti^{4+} in TiO_2. This indicates that the amount of Ti^{3+} ions on the surface of reduced TiO_2 was too small to analyze by XPS. In contrast, there was a
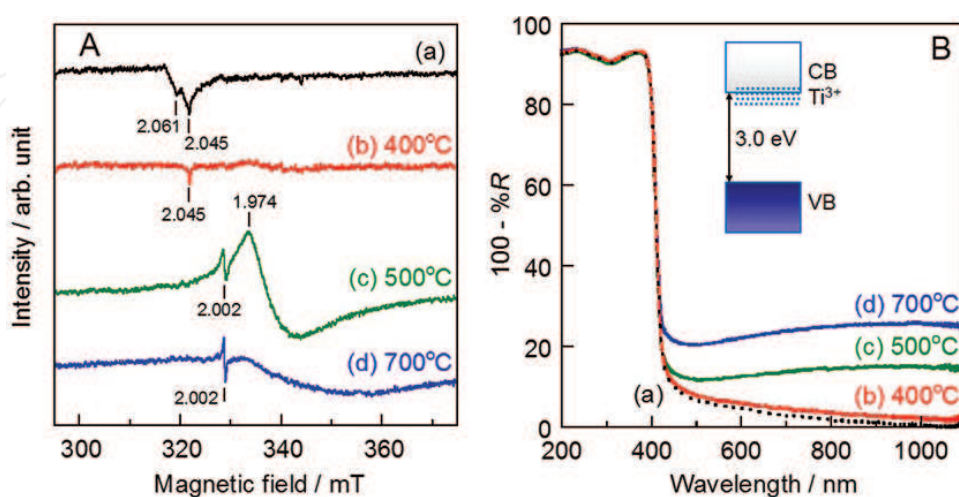
Figure 4. (A) ESR spectra and (B) diffuse reflectance UV-vis-NIR spectra of H_2-reduced TiO_2 samples: (a) TiO_2 calcined in air at 1100°C, and (b–d) TiO_2 treated with H_2 after calcination at 1100°C. The H_2 treatment temperatures are (b) 400°C, (c) 500°C, and (d) 700°C.
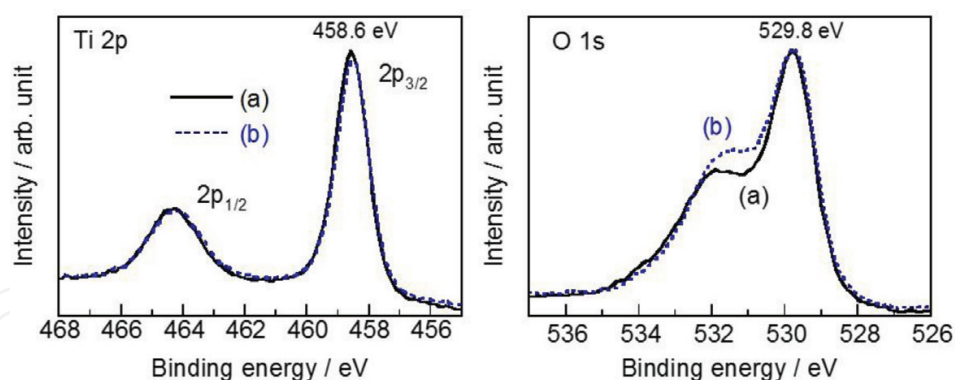
Figure 5. Ti 2p and O 1s X-ray photoelectron spectra of (a) TiO$_2$ calcined in air at 1100°C, and (b) TiO$_2$ treated with H$_2$ at 700°C after calcination at 1100°C.

significant difference observed in the O 1s spectra. The peak at 529.8 eV was assigned to lattice oxygen of TiO$_2$, and the shoulder peak at 531.5–532.0 eV was assigned to surface hydroxyl groups. Unexpectedly, the area assigned to the hydroxyl group was higher in intensity for reduced TiO$_2$ than that of oxidized TiO$_2$. This is because the oxygen vacancies at the top surface became filled by reaction with H$_2$O in the air. It is reported that oxygen vacancies induce dissociation of water molecules and form two hydroxyl groups via H$^+$ transfer to a neighboring lattice oxygen according to Eq. (11) [14]. Therefore, oxygen vacancies are not considered to be present on the surface of reduced TiO$_2$ under ambient conditions. This suggests that oxygen vacancies are not a catalytic site in reduced TiO$_2$ photocatalysts.

$$V_O^{\bullet\bullet} + H_2O + O_O^{\times} \rightarrow 2(OH)_O^{\bullet} \tag{11}$$

4.4. PEC and electrochemical properties

Thermally oxidized TiO$_2$ films were prepared by a simple calcination of a Ti sheet at 900°C [11]. **Figure 6A** shows PEC properties evaluated in dilute sulfuric acid (0.1 mol L^{-1} H$_2$SO$_4$, pH = 1) under UV irradiation (wavelength >330 nm). The thermally oxidized TiO$_2$ film was inactive for
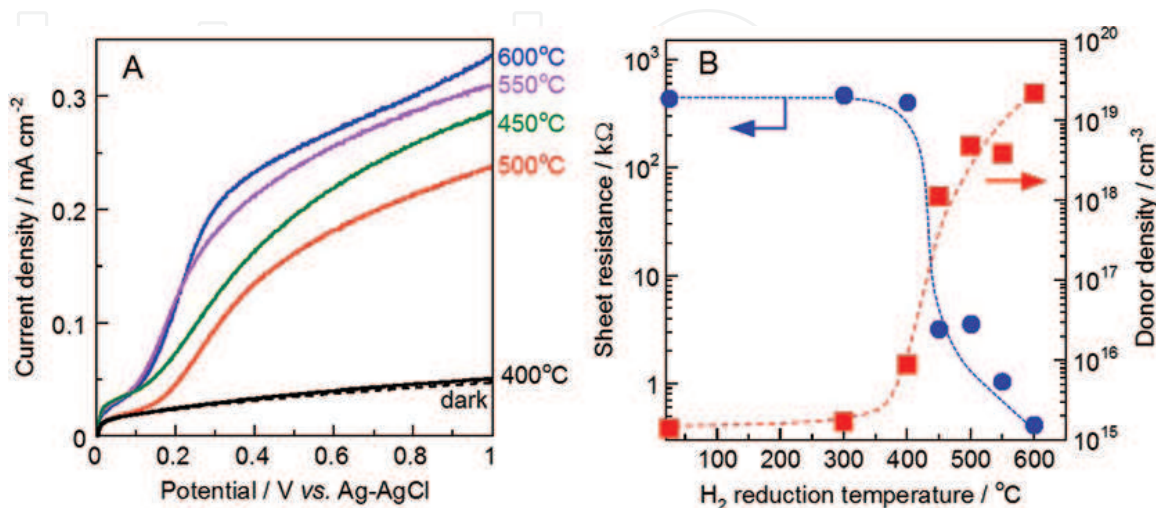
Figure 6. Effect of H$_2$ treatment temperature on (A) PEC voltammetry curves in 0.1 mol L^{-1} H$_2$SO$_4$ (pH = 1) and (B) sheet resistance and donor density of thermally oxidized TiO$_2$ films.

PEC water oxidation. The photocurrent was also negligible for the TiO_2 films treated with H_2 at 400°C. However, anodic photocurrent was observed at applied potentials larger than +0.1 V versus Ag-AgCl after H_2 treatment at higher temperature, suggesting the formation of long-lived holes in the reduced TiO_2 films.

Figure 6B shows the relationship between sheet resistance and donor density of the thermally oxidized TiO_2 films after H_2 treatment [11]. The sheet resistance was measured using a four-point probe. The donor densities were evaluated by Mott-Schottky analysis of the capacitance of the space charge layer. The Mott-Schottky plots of the TiO_2 films showed a positive slope of n-type conductivity. The resistance of the thermally oxidized TiO_2 films was high owing to their low donor density. H_2 treatment at above 450°C greatly reduced the sheet resistance and increased the donor density. H_2 treatment at 600°C increased the donor density by 2–3 orders of magnitude. The enhanced PEC and photocatalytic properties are because of the increase of n-type conductivity by H_2 treatment.

5. Highly efficient TiO_2 photocatalysts for H_2 evolution

### 5.1. Phase junction between anatase and rutile

A mixture of anatase and rutile phases has been reported to be more active than either pure phase alone. Incidentally, the highly efficient commercial photocatalyst Degussa (Evonik) P25 consists of mainly the anatase phase (~80%) with a reasonable amount of rutile (~15%). Because a synergetic effect between anatase and rutile phases is often not observed when separately synthesized powders are simply mixed together, close contact of the phases with each other is expected to be necessary. The high activity of the mixture of phases has been attributed to the separation of photoexcited charge carriers between the two phases. Anatase is considered to be an active component in mixed-phase TiO_2, while rutile is considered to act as an electron sink because of the lower conduction band energy than that of anatase. In contrast, an ESR study revealed that photoexcited electron transfer occurred from the conduction band of rutile to that of anatase in mixed-phase P25 [15]. This would be because the trapping sites of anatase lie below the energy level of the conduction band of the rutile phase. However, in attempts to explain electron transfer from the conduction band of rutile to that of anatase, it is reported that the conduction band of rutile lies ~0.4 eV above that of anatase based on calculation and X-ray photoelectron spectroscopy studies [16]. In this way, there is controversy over the alignment of the conduction band minima of rutile and anatase phases of TiO_2, experimental results suggest that the photoexcited electrons of rutile are less active than those of anatase. It is reputed that pure rutile is less active for photocatalytic H_2 evolution from water than pure anatase and mixed-phase TiO_2.

5.2. Reduced TiO_2 with pure rutile phase

As mentioned, TiO_2 P25 is a well-known commercial material with high photocatalytic activity. The mixture of anatase and rutile phases in P25 is reportedly more active than the individual polymorphs of TiO_2. Contrary to this viewpoint, we demonstrated that H_2-reduced rutile TiO_2 is much more active than mixed-phase P25 for photocatalytic H_2 evolution from

aqueous ethanol solution [17, 18]. To confirm that the anatase phase does not work as an active component, we investigated H_2 reduction treatment of pure single-phase rutile particles [17]. P25 was first calcined in air at 900°C to induce complete phase transition from anatase to rutile, and then the pure rutile phase was reduced by H_2 at 700°C (**Figure 7A**). The photocatalytic H_2 evolution rate was enhanced to 344 μmol h^{-1} after H_2 reduction treatment at 700°C (**Figure 7B**).

Highly efficient rutile photocatalyst is easily fabricated from P25 by H_2 reduction treatment at 700°C for 2 h [18]. The H_2-reduced rutile TiO_2 outperforms anatase-rich TiO_2 because of the wider absorption range caused by its bandgap of rutile (3.0 eV) smaller than that of anatase (3.2 eV). The apparent quantum yield of H_2-reduced rutile TiO_2 was estimated to be 46% for photocatalytic H_2 evolution under 390-nm irradiation, which was 3.3 times higher than that of mixed-phase P25.
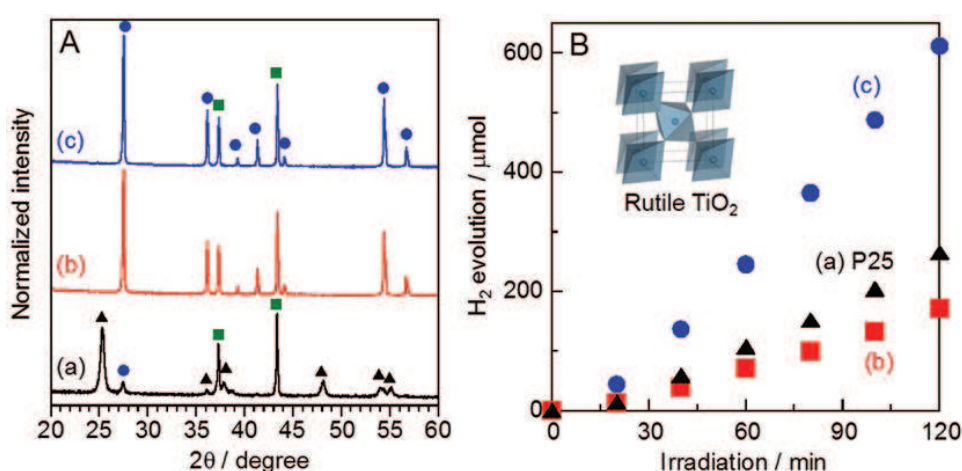
Figure 7. (A) XRD patterns of (a) P25, (b) P25 after calcination at 900°C, and (c) P25 treated with H_2 at 700°C after calcination at 900°C. Symbols ▲, ●, and ■ indicate peaks due to anatase TiO_2, rutile TiO_2, and NiO, respectively, which was added as an internal standard. (B) Photocatalytic H_2 evolution from aqueous ethanol solution over TiO_2 samples (50 mg) with 2.0 wt% Pt under UV irradiation from 380-nm LEDs.

6. Effect of particle size

6.1. Reduced TiO_2 with large particle size

Crystalline size is one of factors affecting the lifetime of photogenerated charge carriers in oxide photocatalysts. For photocatalytic O_2 evolution by water oxidation, anatase TiO_2 nanoparticles exhibit poor activity, while larger rutile particles are more efficient. Large WO_3 particles with low surface area-to-volume ratios are suited to providing long-lived photogenerated holes for water oxidation [19]. This is because slow bulk recombination is the dominant process in larger particles, rather than fast surface recombination.

Controlling the crystalline size of H_2-reduced TiO_2 is expected to improve the photocatalytic activity for O_2 evolution by water oxidation. The crystalline size and electron density of rutile

TiO_2 particles (BET-specific surface are 17 m^2 g^{-1}) was controlled by high-temperature calcination and subsequent H_2 reduction [20]. The photocatalytic activity of TiO_2 for water oxidation was significantly improved by H_2 reduction at 700°C, after calcination at 1100°C (**Figure 8**). The effect of H_2 reduction treatment was obtained only if the rutile particle was previously calcined at temperatures higher than 1000°C. The improved activity was probably due to a combination of the increased crystalline size and the increased electron concentration. The H_2-reduced TiO_2 exhibited high apparent quantum yield for O_2 evolution, 41% under irradiation at 365 nm.

Photocatalytic efficiencies per unit of BET-specific surface area were calculated to consider surface reactivities [20]. The surface reactivity for water oxidation, defined as the O_2 evolution rate per unit of surface area, was significantly improved by H_2 treatment when the samples were previously calcined at >1000°C. It was found that H_2 treatment also improved the surface reactivities for photocatalytic H_2 evolution and photocatalytic CO_2 evolution (oxidative decomposition of acetic acid). The H_2 treatment effectively improved the surface reactivity of TiO_2 calcined at high temperature, without dependence on a particular photocatalytic reaction. Thus, the improvement was not due to the surface modification such as a creation of catalytic active sites, but due to the change of electronic properties.

6.2. Mechanism of the enhanced activity

Figure 9 shows a schematic illustration of the Fermi level in reduced TiO_2. An increase in the electron concentration of n-type semiconductors results in an improvement of the electrical conductivity and an upward shift of the Fermi level toward the conduction band edge [21]. When n-type TiO_2 contacts with water, space charge layer forms at the interface by electron transfer from conduction band, with a simultaneous potential drop inside TiO_2 (**Figure 10**). This is so-called band bending. The higher Fermi level of n-type TiO_2 resulted in the increase of the surface barrier of Schottky type and the electric field in space charge layer. The intrinsic
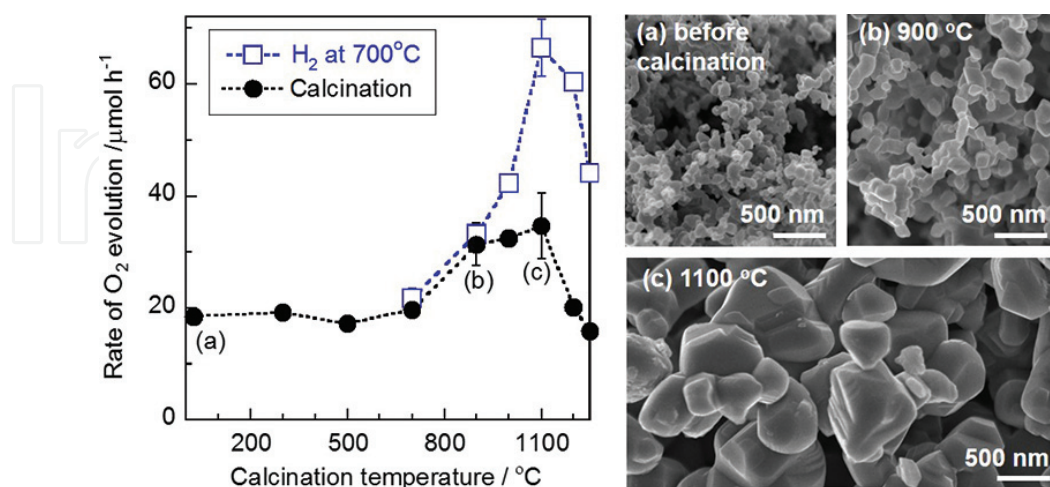

Figure 8. Effect of calcination temperature on the rate of photocatalytic O_2 evolution from water in the presence of sacrificial $AgNO_3$ over TiO_2 samples treated by (●) calcination in air and (□) reduction with H_2 at 700°C after calcination. SEM images of (a) TiO_2 (rutile 96 wt%, BET-specific surface area 17 m^2 g^{-1}), (b) TiO_2 calcined at 900°C, and (c) TiO_2 calcined at 1100°C.
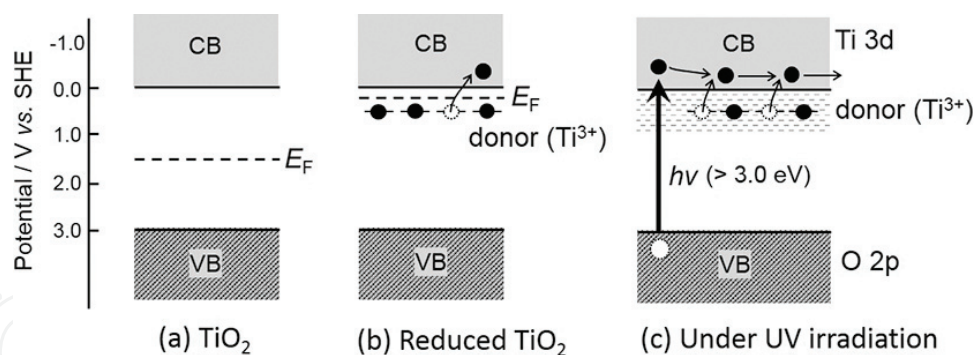
Figure 9. Fermi level (E_F) of (a) stoichiometric TiO$_2$ insulator and (b) reduced TiO$_2$ with n-type conductivity, in which Ti^{3+} ions are donor and (c) reduced TiO$_2$ under photoirradiation.
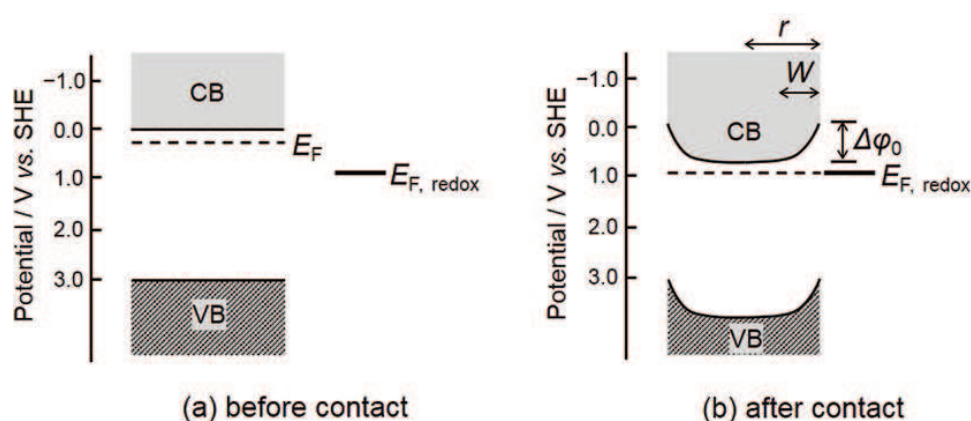
Figure 10. Interface of n-type semiconductor and solution (a) before and (c) after contact in thermal equilibrium. E_{redox} is the electrode potential of redox species in the solution, $\Delta\phi_0$ is potential drop in the semiconductor, W is the width of space charge layer, and r is the radius of the semiconductor particle ($r > W$).

electric field in the space charge layer separates photoexcited electrons and holes, preventing their recombination. This facilitates the transfer of holes from the valence band to the reactants. The width of space charge layer (W) is determined by the donor density (N_D) and the potential drop in the layer ($\Delta\varphi_0$) according to Eq. (12) [21].

$$W = \sqrt{2\varepsilon_0\varepsilon\Delta\phi_0/eN_D}$$ (12)

where ε_0 is the permittivity of vacuum, ε is the dielectric constant of semiconductor, and e is electronic charge. As the electron concentration increases, the space charge layer narrows. Thus, there exist an optimum electron concentration and an optimum particle size depending on this concentration. For example, W can be calculated to be 220 nm at $N_D = 10^{17}$ cm^{-3}, assuming $\Delta\varphi_0 = 500$ mV, and taking ε for rutile to be 86. The radius of photocatalyst particle should be larger than this thickness to obtain a band bending. The calcination temperature dependence observed in **Figure 8** can be explained in terms of the relation between the particle size and the thickness of space charge layer. High-temperature calcination would be necessary to increase the TiO$_2$ particle size to an optimum value, 500 nm–1 μm, to form space charge

layer thickness. The formation of space charge layer is suggested to be involved in the activation mechanism of H_2-reduced rutile TiO_2 with large particle size.

7. Conclusion

H_2 reduction treatment enhanced the photocatalytic activity and PEC properties of rutile TiO_2 with large particle size. One of the most important factors deciding the photocatalytic activity of reduced TiO_2 is the density of electrons in shallow traps and conduction band, rather than the density of oxygen vacancies. H_2 treatment at 500°C created Ti^{3+} ions (trapped electrons), while treatment at 700°C increased the density of conduction electrons, resulting in an improvement of the electrical conductivity of the TiO_2 by 2–3 orders of magnitude. The enhanced activity of the reduced TiO_2 suggests that n-type conductivity governed by electron density plays an important role in suppressing fast recombination by facilitating charge transport. The suppression of recombination in the reduced TiO_2 was caused by not only the high electrical conductivity but also the band bending in space charge layer. The built-in electric field facilitates charge separation and charge transfer. Thus, the surface reactivities of reduced TiO_2 with large particle size were enhanced without dependence on reactions. It was demonstrated that H_2-reduced rutile TiO_2 exhibited photocatalytic activity higher than that of anatase TiO_2 and mixed-phase TiO_2.

Author details

Fumiaki Amano

Address all correspondence to: amano@kitakyu-u.ac.jp

Faculty of Environmental Engineering, The University of Kitakyushu, Wakamatsu-ku, Kitakyushu, Japan

References

[1] Maeda K. Direct splitting of pure water into hydrogen and oxygen using rutile titania powder as a photocatalyst. Chemical Communications. 2013;**49**:8404–8406

[2] Ishihara T, Nishiguchi H, Fukamachi K, Takita Y. Effects of acceptor doping to $KTaO_3$ on photocatalytic decomposition of pure H_2O. The Journal of Physical Chemistry B. 1999;**103**:1–3

[3] Mitsui C, Nishiguchi H, Fukamachi K, Ishihara T, Takita Y. Photocatalytic decomposition of pure water over NiO supported on $KTa(M)O_3$ (M = Ti^{4+}, Hf^{4+}, Zr^{4+}) perovskite oxide. Chemistry Letters. 1999;**28**:1327–1328

[4] Takata T, Domen K. Defect engineering of photocatalysts by doping of aliovalent metal cations for efficient water splitting. The Journal of Physical Chemistry C. 2009;**113**:19386–19388

[5] Karakitsou KE, Verykios XE. Effects of altervalent cation doping of TiO_2 on its performance as a photocatalyst for water cleavage. Journal of Physical Chemistry. 1993;**97**:1184–1189

[6] Zhang Z, Wang CC, Zakaria R, Ying JY. Role of particle size in nanocrystalline TiO_2-based photocatalysts. The Journal of Physical Chemistry B 1998;**102**:10871–10878

[7] Akubuiro EC, Verykios XE. Effects of altervalent cation doping on electrical conductivity of platinized titania. Journal of the Physics and Chemistry of Solids. 1989;**50**:17–26

[8] Amano F, Nakata M, Asami K, Yamakata A. Photocatalytic activity of titania particles calcined at high temperature: Investigating deactivation. Chemical Physics Letters. 2013;**579**:111–113

[9] Chen X, Liu L, Yu PY, Mao SS. Increasing solar absorption for photocatalysis with black hydrogenated titanium dioxide nanocrystals. Science. 2011;**331**:746–750

[10] Wang G, Wang H, Ling Y, Tang Y, Yang X, Fitzmorris RC, Wang C, Zhang JZ, Li Y. Hydrogen-treated TiO_2 nanowire arrays for photoelectrochemical water splitting. Nano Letters. 2011;**11**:3026–3033

[11] Amano F, Nakata M, Yamamoto A, Tanaka T. Effect of Ti^{3+} ions and conduction band electrons on photocatalytic and photoelectrochemical activity of rutile titania for water oxidation. The Journal of Physical Chemistry C. 2016;**120**:6467–6474

[12] Kumar CP, Gopal NO, Wang TC, Wong MS, Ke SC. EPR investigation of TiO_2 nanoparticles with temperature-dependent properties. The Journal of Physical Chemistry B. 2006;**110**:5223–5229

[13] Nowotny MK, Sheppard LR, Bak T, Nowotny J. Defect chemistry of titanium dioxide. Application of defect engineering in processing of TiO_2-based photocatalysts. The Journal of Physical Chemistry C. 2008;**112**:5275–5300

[14] Schaub R, Thostrup P, Lopez N, Lagsgaard E, Stensgaard I, Nurskov JK, Besenbacher F. Oxygen vacancies as active sites for water dissociation on rutile TiO_2(110). Physical Review Letters. 2001;**87**:2661041

[15] Hurum DC, Agrios AG, Gray KA, Rajh T, Thurnauer MC. Explaining the enhanced photocatalytic activity of Degussa P25 mixed-phase TiO_2 using EPR. The Journal of Physical Chemistry B 2003;**107**:4545–4549

[16] Scanlon DO, Dunnill CW, Buckeridge J, Shevlin SA, Logsdail AJ, Woodley SM, Catlow CRA, Powell MJ, Palgrave RG, Parkin IP, Watson GW, Keal TW, Sherwood P, Walsh A, Sokol AA. Band alignment of rutile and anatase TiO_2. Nature Materials. 2013;**12**:798–801

[17] Amano F, Nakata M, Ishinaga E. Photocatalytic activity of rutile titania for hydrogen evolution. Chemistry Letters. 2014;**43**:509–511

[18] Amano F, Nakata M, Yamamoto A, Tanaka T. Rutile titanium dioxide prepared by hydrogen reduction of Degussa P25 for highly efficient photocatalytic hydrogen evolution. Catalysis Science & Technology. 2016;**6**:5693–5699

[19] Amano F, Ishinaga E, Yamakata A. The effect of particle size on the photocatalytic activity of WO_3 particles for water oxidation. The Journal of Physical Chemistry C. 2013;**117**:22584–22590

[20] Amano F, Nakata M. High-temperature calcination and hydrogen reduction of rutile TiO_2: A method to improve the photocatalytic activity for water oxidation. Applied Catalysis B. 2014;**158-159**:202–208

[21] Rajeshwar K. Fundamentals of semiconductor electrochemistry and photoelectrochemistry. In: Licht S, editor. Encyclopedia of Electrochemistry. Semiconductor Electrodes and Photoelectrochemistry. Vol. 6. Weinheim: Wiley-VCH; 2002. pp. 1–53